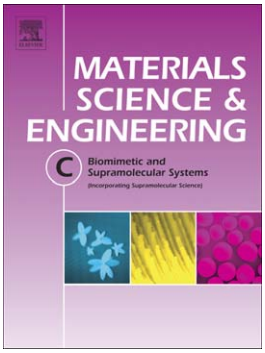

Influence of albumin on the tribological behavior of Ag-Ti (C, N) thin films for orthopedic implants

C.F. Almeida Alves, F. Oliveira, I. Carvalho, A.P. Piedade, S. Carvalho

PII: S0928-4931(13)00537-7
DOI: doi: 10.1016/j.msec.2013.09.031
Reference: MSC 4245

To appear in: *Materials Science & Engineering C*

Received date: 29 April 2013
Revised date: 28 August 2013
Accepted date: 22 September 2013

Please cite this article as: C.F. Almeida Alves, F. Oliveira, I. Carvalho, A.P. Piedade, S. Carvalho, Influence of albumin on the tribological behavior of Ag-Ti (C, N) thin films for orthopedic implants, *Materials Science & Engineering C* (2013), doi: 10.1016/j.msec.2013.09.031

Influence of albumin on the tribological behavior of Ag-Ti (C, N) thin films for orthopedic implants

C. F. Almeida Alves[1*], F.Oliveira[1], I. Carvalho[1], A.P.Piedade[2], S. Carvalho[1]

[1]Universidade do Minho, Departamento Física, Campus de Azurém, 4800-058 Guimarães, Portugal

[2] Grupo de Materiais, Departamento de Engenharia Mecânica, Faculdade de Ciências e Tecnologia da Universidade de Coimbra, 3030-788 Coimbra

ABSTRACT

With the increase of elderly population and the health problems arising nowadays, such as cancer, knee and hip joint prostheses are widely used worldwide. It is estimated that 20% of hip replacement surgeries simply fail after 5 years, due to wear loosening, instability and infection. In this paper it is reported the study of advanced materials with the ability to overcome some of these drawbacks. The development of ceramic coatings, based on carbonitrides of transition metals, such as TiCN, doped with silver, Ag, may represent an effective solution. Thin films of Ag-TiCN were produced by dc reactive magnetron sputtering with silver contents ranging from 4 to 8 at. %. The physical, chemical, structural, morphological/topographical, mechanical and tribological properties were evaluated. The tribological tests were performed in a unidirectional wear simulator, pin on disc, being the antagonists of a ceramic Al_2O_3 ball, and using simulate body fluids as lubricant. Hank's Balanced Salt Solution (HBSS) and bovine serum albumin (BSA) in HBSS were chosen, in order to evaluate the lubrication ability of the solution containing the protein, albumin.

The results revealed that the coatings with Ag content ranging from 4 to 8 at. %, were the most promising, as the tribological properties were superior to the results reported by other authors, which also developed Ag-TiCN coatings containing similar Ag

contents and using similar test conditions. The presence of albumin lead to a lower wear in all the test conditions, and this enhancement was higher in the hydrophobic surfaces.

Keywords: nanostructured coatings, XPS, hydrophobic surface, lubrication limit, critical wetting tension

Highlights: Ag-TiCN coatings were tested tribologically in HBSS and HBSS + BSA fluids. In HBSS lubrication conditions, the tribocorrosion is the wear mechanism responsible for the increase in wear rate, due to the surface reaction with the ionic species of the HBSS solution. All the coatings surfaces show a hydrophobic character, which leads to the protein adsorption to the surfaces and the consequent formation of a protective layer. This layer is responsible for the enhanced tribological behavior detected by the decrease in wear rate. This clearly shows the strong influence of albumin in increasing lubrication limit.

*__Corresponding author.__ Tel.: +351 253 510 470. *Address:* Universidade do Minho, Departamento Física, Campus de Azurém, 4800-058 Guimarães, Portugal. *E-mail address:* alves.cristiana89@gmail.com

1. INTRODUCTION

The number of hip arthroplasties has been growing in recent years as a result of increased life expectancy of the world population. The development of materials with the ability to reduce the number of revision arthroplasties is an emerging field, thus contributing to reduce the costs associated with these surgical procedures and above of all to improve of patient´s life quality. Considering the aggressive environmental conditions to which they are subjected to, these materials must meet several

requirements, namely: biocompatibility, wear and corrosion resistance and resistance to microbial colonization [1]. The development of ceramic coatings, such as DLC [2], transition metal (e.g. Ti, Zr) carbides [3, 4], nitrides [5, 6] and carbonitrides [7], has been perceived as one of the solutions able to increase the lifetime of orthopedic prosthesis. TiCN coatings are able to comprise low wear rates, low friction coefficients [8] and good corrosion resistance [9], which makes them good candidates for orthopedic implant applications. Despite the major developments in biomaterials field, microbial colonization of the implant surface and consequent infection remains an unsolved problem. In order to overcome this limitation great efforts have been dedicated to the development of biodevices with antibacterial surfaces, being most of them based on the incorporation of Ag nanoparticles [10, 11]. Moreover, it is reported that the incorporation of small amounts Ag in TiN [12], CrN [13], ZrN [14], DLC [15] and TaN [16] matrixes is able to reduce the friction coefficient and improve the wear resistance of the base coating, due to the lubricant properties of this metal. Sánchez-lópez [10] claimed that the incorporation of Ag up to 6 at. % promoted an increase in the TiCN wear resistance. However, for higher Ag contents an opposite trend was reported. Similar results were also found for Ag-TiN, Ag-CrN and Ag-ZrN coating [13]. Furthermore, the addition of high contents of Ag may induce cytotoxicity in the host tissue and consequent rejection of the biomaterial [17]. Also, the incorporation of higher Ag contents promotes the increase in Ag clusters size, thus reducing the surface area and consequently their antimicrobial effect [9]. In this sense, the amount of Ag incorporated in the coatings must be tailored in order to obtain good tribological properties, good corrosion resistance, biocompatibility and antibacterial properties. According to previous studies [9, 10] the best compromise for Ag-TiCN coatings were obtained for Ag contents up 6 at. % .

Synovial joints are protected from external agents by articular capsules, containing synovial membrane and synovial fluid, whose role is to maintain the balance between secretion and adsorption of the fluid [18]. This fluid has an extreme complex chemical composition, being mainly composed of an electrolytic solution rich in proteins (mainly albumin), polysaccharides (hyaluronic acid) and water-solved compounds. Hyaluronic acid is claimed to guarantee a high degree of viscosity, which enables a hydrodynamic lubrication, while albumin is able to increase the lubrication when adsorbed on the surface of joint material. Some studies [19] performed *in vitro* studies which evaluated the effect of few synovial fluid components, with a special focus on: bovine serum albumin (BSA); hyaluronic acid (HA) and phospholipids suspensions. Each of these components is usually included in a solution with an ionic composition that is similar to the one found in biological fluids, such as Hank's Balanced Salt Solution (HBSS).

In the present study the wear behavior of Ag-TiCN coatings was evaluated for different Ag contents ranging from 0 to 8 at. %. In order to simulate the conditions present in the synovial joints, the tribological tests were performed in a pin-on-disk tribometer for the following conditions: i) without lubrication, ii) using Hank´s Balanced Salt Solution (HBSS) as lubrication medium, and iii) using HBSS solution and bovine serum albumin (BSA) as lubrication medium. The objective of this work was to study the effect of albumin in tribological behavior.

2. EXPERIMENTAL DETAILS

Ag-TiCN coatings were deposited by reactive dc magnetron sputtering from a high-purity Ti target (200x100 mm^2) and a composed Ag-Ti target onto polished and ultrasonically cleaned 316L stainless steel (20x20 mm^2) and single crystalline silicon (100) (1x1 mm^2). In order to produce Ag-TiCN coatings, 8 Ag nuggets were

incorporated on the Ti target, resulting in this composed Ag-Ti target in a relative Ag/Ti erosion area of 22%. To further vary the Ag content in the films the current density applied to each target was varied as indicated in table 1. The substrates were previously sputter-etched for 20 min in an Ar atmosphere at constant current density of 10 mA/cm^2 and Ar flow of 60 sccm. The depositions were carried out in Ar+C_2H_2+N_2 atmosphere, with the substrates rotating at 70 mm over the target at constant speed of 8rpm. The base pressure in the deposition chamber was 1.4x10^{-3} Pa, the films were grown at a constant temperature (373 K) and with an applied bias voltage of -50 V. Argon flow was kept constant at 60 sccm while the reactive gases fluxes, C_2H_2 and N_2, were adjusted (in a range of 5.5 – 7 sccm) as can be depicted in table 1.

The chemical composition of all surfaces was assessed by electron probe micro analysis (EPMA) using a Cameca, Camebax SX 50 equipment, operating at 10kV and 40 nA. Ball crater tests were used to measure the film thickness. The structure and phase distribution of the films were determined by X-ray diffraction (XRD), Raman spectroscopy and X-ray photoelectron spectroscopy (XPS). XRD analysis of the coatings deposited on Si, was performed using a Philips X'Pert, at 40 kV and 35 mA, with Co radiation ($\lambda k_{\alpha 1}$=0.178896 nm and $\lambda k_{\alpha 2}$=0.179285 nm), equipped with collimator and Bragg–Brentano geometry. All the tests were performed with a step size of 0.025º and a time per step of 0.5 s, in 20–120 º range. Raman spectra were acquired in a Renishaw 2000 apparatus, operating with an Ar laser (514.5 nm) and the spectra were acquired in a range of 150-2000 cm^{-1}. The XPS analyses were performed in a VG–ESCLAB 250iXL spectrometer. The pressure in the analysis chamber was kept below 5×10^{-8} Pa and the analysis were performed using monochromatic radiation Al–Kα (hν=1486.92 eV). The photoelectrons were collected with an angle of 90^o with respect to the surface of samples. The energy step was of 20 eV for the survey spectra and of

0.05 eV for the high-resolution spectra. The C1s line at 285.0 eV (hydrocarbon peak) was used to calibrate the binding energies. The XPS was also used for the in-depth analysis of the thin films by sputtering the surface with 3keV Ar+ beam. The chemical compositions were obtained using the sensitivity factor of the Scofield library.

The morphology/topography of the coatings, was evaluated by atomic force microscopy (AFM) using a NanoScopeIII a model from Digital Instruments operating in tapping mode. AFM images were taken over scanning areas of 10 x 10 μm^2. The wettability characteristics of the surfaces were assessed by measuring the static contact angle with 10 µl of distilled and deionized water, glycerol and formamide in a DataPhysics QCA-20 apparatus. For each sample, a minimum of seven measurements was taken, after allowing the system (air/water/surface) to reach equilibrium, and the average value was calculated.

The hardness and the Young modulus were measured by nanoindentation test (Micro Materials Nano Test) using a Berkovich indenter. The normal stylus load was 10 mN and the results are the average of 15 independent indentations.

The tribological properties of Ag-TiCN coatings were studied using a pin-on-disc tribometer. All the tribological measurements were performed at identical conditions: 10615 laps at 1 Hz, total distance of 500 m, normal load 2 N, linear speed 50 mm/s, counterpart Al_2O_3 ball with a diameter of 10 mm, room temperature and relative air humidity of 35%. All coatings underwent testing at three different conditions: dry sliding in humid air, lubricated sliding in HBSS solution and lubricated sliding in a HBSS + BSA solution, which is the most common lubricant used to reproduce synovial liquids. The concentration of BSA used in all tribological tests was 10 g/l, in agreement with literature [20]. The tribological performance was examined with respect to the wear rates of the coating. The coating wear rate was evaluated on the basis of profile

measurements on the wear track. The wear rates were determined according to ASTM G 99-04 (2004) Standard Test Method for Wear Testing with Pin-on-Disk Apparatus. In order to evaluate the dominant wear mechanism, the wears tracks were studied using 3D profilometry (Mahr RM600-S).

3. RESULTS AND DISCUSSION

3.1. Physical and chemical characterization

The deposition parameters, the chemical composition, the thickness and some mechanical properties of the coatings are summarized in table 1. The deposition rate ranged from 1.1 to 1.6 µm increasing with the current density applied to both targets. (J_{Ti+Ag} + J_{Ti}). Although a decrease on the density applied to the Ti target and an increase on the density on the TiAg target are observed, the sum of current densities applied to both targets is increasing. To justify the increased deposition rate one should take into account the increase on the sum of current density applied to both targets, which corresponds to an increase in ion bombardment and proportionally the amount of ejected atoms. The elemental chemical composition shows that by increasing the J_{TiAg}/J_{Ti} current density ratio, the Ti content in the coatings decreases from 37 to 21 at. % along with an increase in the Ag content from 0 to 8 at. %. The N content decreases slightly from 31 to 24 at. % and the C content increases from 28 to 42 at. %. In fact, the Gibbs free energy for the formation of TiN phases is -290 kJ/mol and for TiC is -180 kJ/mol. Therefore with decreasing Ti content an increase on the carbon content is observed since there is a clear trend to the formation of thermodynamically more stable

carbon phases [9]. In order to confirm these assumptions, XPS analysis on the coating with lowest Titanium content and consequently highest Carbon content was performed. Figure 1 shows the (a) Ti 2p, (b) C 1s, (c) N 1s and (d) Ag 3d core level XPS spectra of Ag8TiCN coatings. On the XPS analysis the Ti2p spectra (figure 1.a) there are identified two doublets (Ti2p3/2 and Ti2p1/2 separated by 5.8eV). The first contribution can be associated to TiCN (electron binding energies at 455.3 and 461.1 eV) bonds, since according to the literature, these binding energy are a commitment between TiN (electron binding energy 455.4 and 461.2 eV) and TiC (electron binding energy 454.6 and 460.4 eV) phases. However, in the following discussion it will refer to them as a Ti-C-N phase. Also, these bindings energies for titanium are consistent with the C-Ti and N-Ti bonds observed at the C1s (282.7 eV) and N1s (497.1 eV) XPS spectra of figure 1.b and d, respectively. Furthermore, there is evidence of the graphitic C-C bond at 284.9 eV and the presence of C-N bond at 287.5 eV on C1s spectra. The last bond is confirmed on N1s XPS spectra where there is evidence of the N-C bonds at 398.5 eV. Within the O1s XPS spectra it is evident the appearance of the peak centered at 531.1 eV reported for O-Ti bonds. This is consistent by Ti2p spectra when appear the TiO_x bond at 456.9 and 462.7 eV. The oxygen presence is due to the residual oxygen in the vacuum chamber, in the targets and also due to contamination after deposition [9, 10]. Finally, the fitting of Ag3d XPS spectra (figure 1.c) revealed two doublet (Ag3d5/2 and Ag3d3/2 separated by 6eV) related to the Ag-Ag metal bonds (368.6 and 374.6 eV) and another one assigned to Ag-clusters bonds (369.1 and 375.1 eV), which was somehow predictable due the low solubility of C and N in silver. In agreement with Lopez-Salido [21], for Ag nanoparticles with approximately 2 nm diameter a high core level shift of 0.6 eV is observed when compared to bulk Ag crystals. For metals, the change from bulk to clusters with sizes lower than 4 nm, induces a decrease in the binding energy of

the core levels due to a decrease in the core-hole screening by conduction electrons, as a result of the discretization of the conduction band. This results in positive shifts and in increased line-width of the peaks. The positive core level shift can also be attributed to higher electronegativity of the neighbor's specimens. These results are consistent with others authors [21, 22].

The measured contact angle values in water, glycerol and formamide, of the samples are presented in table 2. More important than the determination of the static contact angle values between a surface and a pure liquid, is the determination of the surface critical wetting tension (γ_c) with a homologous series of liquids, calculated by the Zisman-plots. The results of the different surfaces are presented in table 2 and indicate that the incorporation of Ag induces a decrease of γ_c. In fact, when considering only the contact angle with water, the results seem to point out to less hydrophobic surfaces due to the incorporation of silver. However, the roughness of the sample with higher Ag content is lower than that of the two other surfaces (Table 3) and consequently the results must be considered as comparative and not as absolute value. Nevertheless, the overall trend is that the incorporation of Ag induces a decrease of the critical wetting tension, indicating a greater difficulty of the coatings to be completely wet by liquids with high critical tension, such as water (γ_L= 72 mJ/m^2).

3.2. Structural characterization

XRD analysis was carried out in order to understand the evolution of the structure with the Ag content. The XRD patterns are shown in figure 2.a and the main identified crystalline phases are $TiC_{0.3}N_{0.7}$ (ICDD card no 00-042-1488) (face centered cubic) and Ag (ICDD card no 00-004-0783) which is in agreement with XPS analysis. The differences in the chemical composition correlate well with the differences observed in

the developed structure. For the sample without Ag, the films crystallize in a B1-NaCl fcc structure typical for $TiC_{0.3}N_{0.7}$, although a peak shift towards lower angles is observed. This fact is in agreement with the measured chemical composition, because these samples contain a slightly higher C/N atomic ratio than $TiC_{0.3}N_{0.7}$. The deposition process is associated with the development of the compressive stresses, which may also explain the shift towards lower angles. This stress is due to the deposition parameters, namely, the bombardment during film growth. Since the deposition typically occurs at low temperature, the mobility of adsorbed species is low , and thus cannot undo the effect mentioned above.

The samples with low Ag percentage present a new diffraction peak attributed to Ag (111) fcc structure. The silver phase causes a peak shift of the $TiC_{0.3}N_{0.7}$ phase towards high angles induced by a relaxation of residual compressive stress as reported by Manninen [9]. However, as the decrease in Ti content is not accompanied by a similar trend for N content, this shift can also be ascribed to a continuous decrease of the titanium bonded to carbon. The increment in the Ag content leads to a loss of the XRD peak intensity and a decrease on the crystal size of the TiCN phase. The grain size of TiCN and Ag phases was determined by Scherrer formula considering the (111) peak, for both crystalline phases. The calculated values are presented in figure 2.b. These changes can be understood as a consequence of the interruption of the growth of the TiCN phase by nucleation of Ag nanocrystals and/or by the presence an amorphous phase. In fact, the low Ti(C+N) atomic ratio suggests the presence of an additional XRD amorphous phase, most likely of a-C or a-CN_x type. The presence of this amorphous phase was confirmed by XPS analysis. Also Raman spectroscopy as carried out with aim to obtain further information regarding these a-C and/or a-CN_x phase.

Raman spectroscopy was performed on the Ag4TiCN coatings, deposited on 316L stainless steel substrates. The Raman spectrum obtained from two different points of the Ag4TiCN as deposited sample presented in figure 3, is dominated by the presence of the D and G bands at 1388 and 1581 cm^{-1} respectively, corresponding to the presence of the sp^2 C-C bonds. According to Dreiling [23] TiN presented four peaks at approximately 225, 315, 450 and 550 cm^{-1}, and four peaks to TiC located at 280, 385, 585 and 675 cm^{-1} identified by Raman spectroscopy. In this specific case, Ag4TiCN coating, it seems that the TiCN bonds should be located between TiN and TiC peaks. Nevertheless, the Raman band around 535 cm^{-1} is associated of the presence of TiO_2 bonds, confirming the XPS results [9].

Figure 4 shows AFM images of the Ag-TiCN films deposited on stainless steel. In the images it is possible to see the morphology developed in each film, showing that they exhibit a columnar structure, which is confirmed by the cross section SEM micrograph inset on the AFM image of Ag8TiCN coating. When Ag is added to the coating, the surface morphology of the coatings evolves to cauliflower-like patterns, which results in a decreasing on surface roughness [24]. However with the increase of the Ag content (4 % at. to 8 % at.) the cauliflower patterns are smoothed. This structure is formed when diffusion is low, resulting from the depositions parameters in particular the low ion bombardment and/or low deposition temperature. The roughness is a consequence of the morphology and the differences observed in all samples on the Sa roughness is due to the appearance of a second phase, Ag. According to the literature the Ag tends to diffuse to the surface and segregate to the column's boundaries promoting a decrease on the surface roughness [12, 25].

3.3. Mechanical characterization

The hardness and Young's modulus values are presented in table 1. The hardness varied in a range from 14 to 16 GPa, much lower than the typical values reported for pure TiCN coatings, ranging from 30 to 36 GPa [26-28]. These overall lower values are related with microstructural and chemical composition aspects. In fact, low energetic conditions of the deposition (low negative substrate bias and low deposition temperature) can lead to columnar and open morphologies. The presence of the O also promotes a decrease in the hardness, as it was already discussed on Veprek [29]. The mechanical properties are also affected by phase composition of these nanocomposites influencing the balance between hard and soft phases and their distribution – nc-TiCN/nc-Ag/a-CN_x. Further discussion regarding the dependence can be found elsewhere [10, 30].

3.4. Tribological characterization

The tribological performance of the Ag-TiCN coatings against Al_2O_3 was investigated without lubrication (dry) and using HBSS and HBSS+BSA solutions as lubricants. Figure 5 presents the wear rate values for the coatings for different lubrication solutions. The prevailing wear mechanism is abrasion, as seen in the inset of figure 5. Starting with the results achieved on dry conditions, despite the low hardness and Young´s modulus for the Ag-TiCN coatings the wear rates are in $1.52x10^{-7}$ and $2.12x\ 10^{-7}$ mm^3/Nm range. These results demonstrate that the wear rate is slightly reduced for low silver content, while for higher Ag contents the wear rate increases. This behavior was already found by several authors. Endrino [31] made similar observation with TiC-Ag films. These authors found a slightly decrease on the wear volume in the samples with Ag content up to 10 at. %. Also Basnyat [32] established 5 at. % Ag on CrAlN films as

optimal content for wear resistance. Also Jurci and Dlouhý [33] discussed the self-lubricating effect of the Ag on CrN films, mainly at high temperatures. The incorporation of Ag in the coatings with a decrease on the Ti content (without significant changes on the N content) creates a situation where it is more favorable for the carbon to form graphite than the TiCN fcc structure. This means that not only the silver phase controls the wear rate, but also that the a-C and/or a-CN_x phase promote wear rate variations too. However, further increase on the Ag content, promotes a decrease on the wear resistance. The high atomic % of a-C with the higher content of Ag may adversely affect the wear behavior of the sample as both the previous phases are self-lubricated but also very soft. These results are similar to those of other authors such as Sánchez-López [10]. The compromise between these two phases can be positive for Ag content up to 4 at. % and become negative for higher levels of silver. Therefore the content of a-C also increased and the previously beneficial commitment ceases to exist. On dry conditions, it seems that the wear rate is related with TiCN/nc Ag/a-CNx ratio.

On HBSS lubrication conditions, the tribocorrosion is the wear mechanism responsible for the increase in wear rate. In fact, the electrolyte characteristic of this lubricant is capable of inducing oxidation of the metallic elements present in the modified surfaces which in turns is responsible for the increase of the wear rate. Moreover, this increase is proportional to the decrease of the contact angle of the surfaces with water. Lowest contact angles indicate better wettability of the surface by water and aqueous solutions and, consequently, increased reaction with the ionic species of the HBSS solution.

In case the HBSS+BSA environment the albumin protects the surface resulting in a decrease of the wear rate (figure 5). In fact, figures 6 and 7 show the in depth XPS spectra for the sample Ag8TiCN in dry environment and in HBSS+BSA lubricated

situation, respectively. Comparing the two spectra, it is visible that the contact of the surface with HBSS and protein (HBSS+BSA) results on surface modification. As it is possible to observe on the figure 7, a layer with constant composition, TiCN(O), for the first 500 nm depth, which appears to protect tribologically the coating surface against wear.

The protective nature of the protein on the surface is highlighted on sample Ag8TiCN. In fact, the decrease observed in the wear rate when BSA is added to HBSS is much higher in this coating than in the other two surfaces. This fact is explained by the lowest γ_c of Ag8TiCN. The adsorption of proteins onto surfaces with lower critical surface tension is thermodynamically favorable, as it is not necessary for the protein to overcome the barrier of the well-structured three dimensional layers of water molecules present in surfaces with higher surface energy. The adsorption of higher protein concentrations implies that the denaturation of this biological compound, that occurs due to the mechanical solicitation of the tribological test, forms a continuous layer of albumin in its secondary structure repealing the aqueous solution and thus preventing its harmful effect [18, 34].

4. CONCLUSION

Ag-TiCN coatings were deposited by dc reactive magnetron sputtering with variable silver content (0 to 8 at. %). The samples crystallized in a B1-NaCl crystal structure typical of $TiC_{0.3}N_{0.7}$. With the increase in Ag content a second crystalline phase begins to appear promoting a reduction in the TiCN grain size. Simultaneously, amorphous carbon-based phases begin to appear, also confirmed by Raman spectroscopy and XPS. It was evaluated the tribological performance of these coatings against Al_20_3 counterpart, in environments that simulate the biological environment (HBSS) where

prostheses are inserted, having been highlighted the importance of the study of the influence of albumin (majority constituent of synovial liquid). Typically the samples have shown a hydrophobic character, however the incorporation of Ag induced a slight decrease in hydrophobicity. This property provides the protein adsorption to the surfaces leading to formation of a protective layer, which promotes an enhanced tribological behavior observable by decreased in wear rate. This clearly shows the strong influence of albumin in increasing lubrication limit. In fact the results achieved with the pair Al_2O_3/Ag-TiCN for silver content with 8 at. % were very promising.

Acknowledgments

This research is sponsored by FEDER funds through the program COMPETE – Programa Operacional Factores de Competitividade – and by national funds through FCT – Fundação para a Ciência e a Tecnologia –, in the framework of the Strategic Projects PEST-C/FIS/UI607/2011", and PEst-C/EME/UI0285/2011 and under the project , PTDC/CTM/102853/2008.

5. REFERENCES

[1] C. Oliveira, L. Gonçalves, B. Almeida, C. Tavares, S. Carvalho, F. Vaz, R. Escobar_Galindo, M. Henriques, M. Susano, R. Oliveira, Surface and Coatings Technology, 203 (2008) 490-494.

[2] D. Caschera, F. Federici, S. Kaciulis, L. Pandolfi, A. Cusmà, G. Padeletti, Materials Science and Engineering: C, 27 (2007) 1328-1330.

[3] T. Polcar, T. Vitu, L. Cvrcek, R. Novak, J. Vyskocil, A. Cavaleiro, Solid State Sciences, 11 (2009) 1757-1761.

[4] K. Balázsi, M. Vandrovcová, L. Bačáková, C. Balázsi, Materials Science and Engineering: C, 33 (2013) 1671-1675.

[5] M. Gispert, A. Serro, R. Colaco, A. do Rego, E. Alves, R. Da Silva, P. Brogueira, E. Pires, B. Saramago, Wear, 262 (2007) 1337-1345.

[6] D. Zhang, W. Zeng, Z. Zi, P.K. Chu, Materials Science and Engineering: C, 29 (2009) 1599-1603.

[7] M. Gispert, A. Serro, R. Colaço, E. Pires, B. Saramago, Wear, 263 (2007) 1060-1065.

[8] J. Hsieh, C. Li, W. Wu, A. Tan, Journal of Materials Processing Technology, 140 (2003) 662-667.

[9] N. Manninen, R.E. Galindo, N. Benito, N. Figueiredo, A. Cavaleiro, C. Palacio, S. Carvalho, Journal of Physics D: Applied Physics, 44 (2011) 375501.

[10] J. Sánchez-López, M. Abad, I. Carvalho, R. Escobar Galindo, N. Benito, S. Ribeiro, M. Henriques, A. Cavaleiro, S. Carvalho, Surface and Coatings Technology, 206 (2012) 2192-2198.

[11] P. DeVasConCellos, S. Bose, H. Beyenal, A. Bandyopadhyay, L.G. Zirkle, Materials Science and Engineering: C, 32 (2012) 1112-1120.

[12] P. Kelly, H. Li, K.A. Whitehead, J. Verran, R. Arnell, I. Iordanova, Surface and Coatings Technology, 204 (2009) 1137-1140.

[13] P. Kelly, H. Li, P. Benson, K. Whitehead, J. Verran, R. Arnell, I. Iordanova, Surface and Coatings Technology, 205 (2010) 1606-1610.

[14] E. Silva, M. Rebelo de Figueiredo, R. Franz, R. Escobar Galindo, C. Palacio, A. Espinosa, S. Calderon V, C. Mitterer, S. Carvalho, Surface and Coatings Technology, 205 (2010) 2134-2141.

[15] J. Endrino, R. Escobar Galindo, H.-S. Zhang, M. Allen, R. Gago, A. Espinosa, A. Anders, Surface and Coatings Technology, 202 (2008) 3675-3682.

[16] J. Hsieh, T. Yeh, C. Li, C. Chiu, C. Huang, Vacuum, (2012).

[17] A. Betts, D. Dowling, M. McConnell, C. Pope, Materials & design, 26 (2005) 217-222.

[18] A. Serro, M. Gispert, M. Martins, P. Brogueira, R. Colaco, B. Saramago, Journal of Biomedical Materials Research Part A, 78 (2006) 581-589.

[19] M. Gispert, A. Serro, R. Colaco, B. Saramago, Wear, 260 (2006) 149-158.

[20] B.D. Ratner, A.S. Hoffman, F.J. Schoen, J.E. Lemons, Biomaterials Science, 484 (1996).

[21] I. Lopez-Salido, D.C. Lim, Y.D. Kim, Surface science, 588 (2005) 6-18.

[22] N. Figueiredo, N. Carvalho, A. Cavaleiro, Applied Surface Science, 257 (2011) 5793-5798.

[23] I. Dreiling, A. Haug, H. Holzschuh, T. Chassé, Surface and Coatings Technology, 204 (2009) 1008-1012.

[24] Y. Pei, D. Galvan, J.T.M. De Hosson, Acta Materialia, 53 (2005) 4505-4521.

[25] C. Tseng, J. Hsieh, S. Jang, Y. Chang, W. Wu, Thin Solid Films, 517 (2009) 4970-4974.

[26] S. Bull, D. Bhat, M. Staia, Surface and Coatings Technology, 163 (2003) 499-506.

[27] D. Martínez-Martínez, C. López-Cartes, A. Justo, A. Fernández, J. Sánchez-López, Solid State Sciences, 11 (2009) 660-670.

[28] C. Mulligan, T. Blanchet, D. Gall, Surface and Coatings Technology, 203 (2008) 584-587.

[29] S. Veprek, P. Karvankova, M.G. Veprek-Heijman, Journal of Vacuum Science & Technology B: Microelectronics and Nanometer Structures, 23 (2005) L17-L21.

[30] S. Carvalho, L. Rebouta, E. Ribeiro, F. Vaz, C. Tavares, E. Alves, N. Barradas, J. Riviere, Vacuum, 83 (2009) 1206-1212.

[31] J.L. Endrino, J.J. Nainaparampil, J.E. Krzanowski, Surface and Coatings Technology, 157 (2002) 95-101.

[32] P. Basnyat, B. Luster, Z. Kertzman, S. Stadler, P. Kohli, S. Aouadi, J. Xu, S. Mishra, O. Eryilmaz, A. Erdemir, Surface and Coatings Technology, 202 (2007) 1011-1016.

[33] P. Jurči, I. Dlouhý, Applied Surface Science, 257 (2011) 10581-10589.

[34] C. Morillo, Y. Sawae, T. Murakami, Tribology International, 43 (2010) 1158-1162.

Figure Captions:

Figure 1: XPS spectra of (a) Ti2p, (b) O1s, (c) C1s, (d) N1s and (e) Ag3d of Ag-TiCN coatings deposited by dc reactive magnetron sputtering, at 900nm in depth.

Figure 2: (a) XRD patterns of the Ag-TiCN coatings deposited by reactive magnetron sputtering, with different Ag/Ti atomic ratios. (b) Grain size of TiC0.3N0.7 as a function of % at Ag.

Figure 3: Raman spectra of the Ag4-TiCN as deposited.

Figure 4: AFM topographic 3D maps of the TiCN and Ag-TiCN films deposited by reactive magnetron sputtering (scans of 10 x 10 μm^2; z-scale 1 µm/division)**.**

Figure 5: Wear rate of coating when Al2O3 is counter-body of the three environments.

Figure 6: XPS in-depth analysis of the sample Ag8TiCN on dry conditions of lubrication.

Figure 7: XPS in-depth analysis of the sample Ag8TiCN lubricated by HBSS+BSA.

Table 1: Chemical composition, deposition parameters, thickness, hardness and Young's modulus of the deposited samples.

Sample	Chemical composition [% at.]					$Ø_{C2H2}$ [sccm]	$Ø_{N2}$ [sccm]	J_{Ti} [mA/cm^2]	J_{TiAg} [mA/cm^2]	J_{TiAg}/J_{Ti} [mA/cm^2]	Deposition Rate [µm/h]	Thickness [µm]	Hardness [GPa]	Young's modulus [GPa]
	C	N	O	Ti	Ag									
TiCN	28	31	4	37	0	6	6	10	0	0	1.3± 0,06	2.1±0 .06	15±1 .1	232 ±28
Ag4 TiCN	33	30	3	30	4	7	7	10	2.5	0.25	1.6± 0,04	2.0±0 .04	16±1 .5	214 ±33
Ag8 TiCN	42	24	5	21	8	5.5	5.5	5	3.75	0.75	1.1± 0,05	1.8±0 .05	14±1 .5	154 ±14

Table 2: Contact angle mean values and critical wetting tension of the TiCN and Ag-TiCN films.

Sample	Contact angle, θ [°]			γ_c [mJ.m^{-2}]
	Water	Formamide	Glycerol	
TiCN	112±3	61±2	80±2	49.3
Ag4 TiCN	90±2	74±2	82±1	30.2
Ag8 TiCN	75±2	64±2	68±3	14.8

Table 3: Sa, Sq and Sms roughness values of the TiCN and Ag-TiCN coatings.

Sample	TiCN	**Ag4**TICN	**Ag8**TiCN
Sa [nm]	67±2	66±9	36±6
Sq [nm]	89±3	85±9	42±6
Smáx [nm]	680±7	707±12	418±7

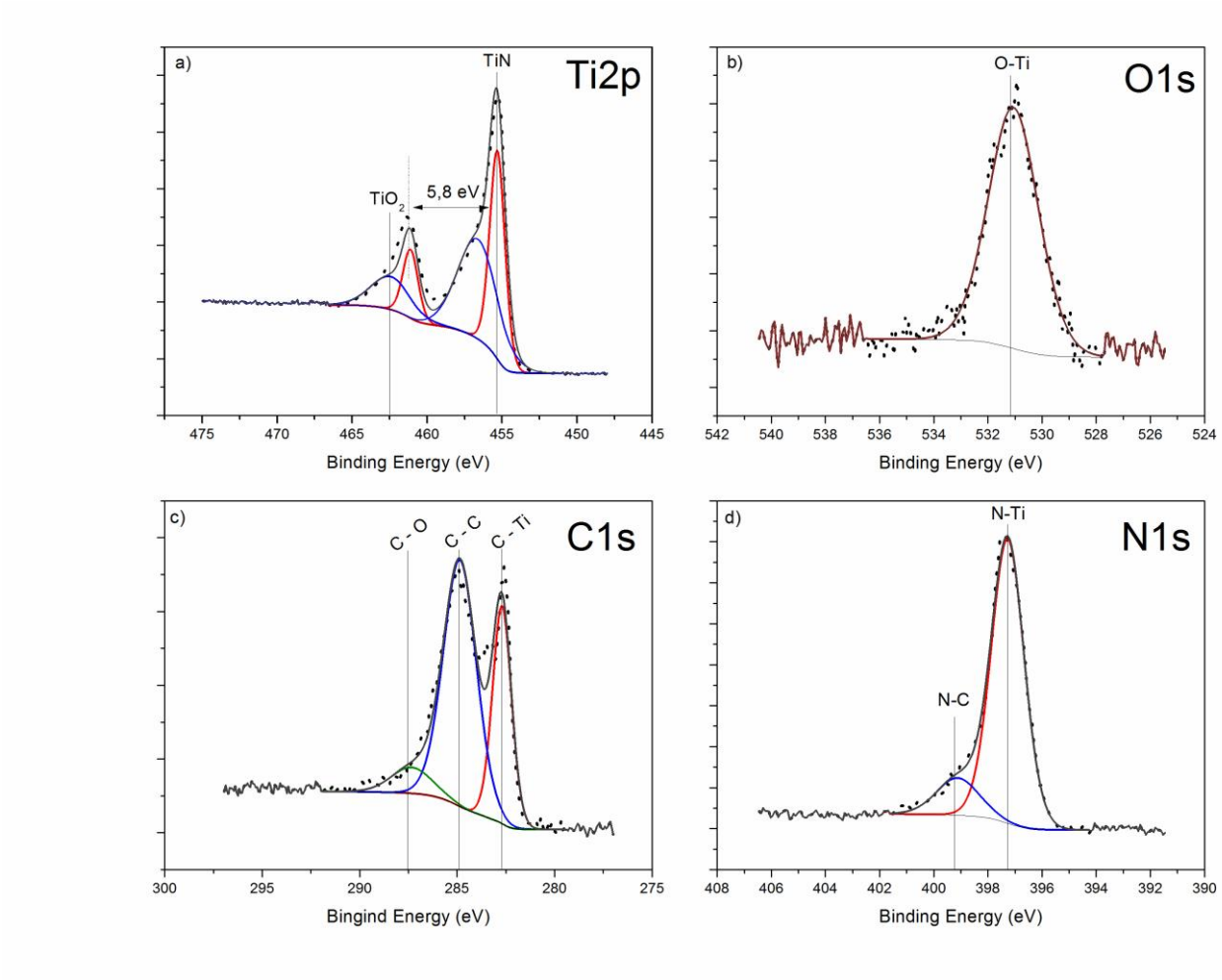

Figure 1.a,b,c,d

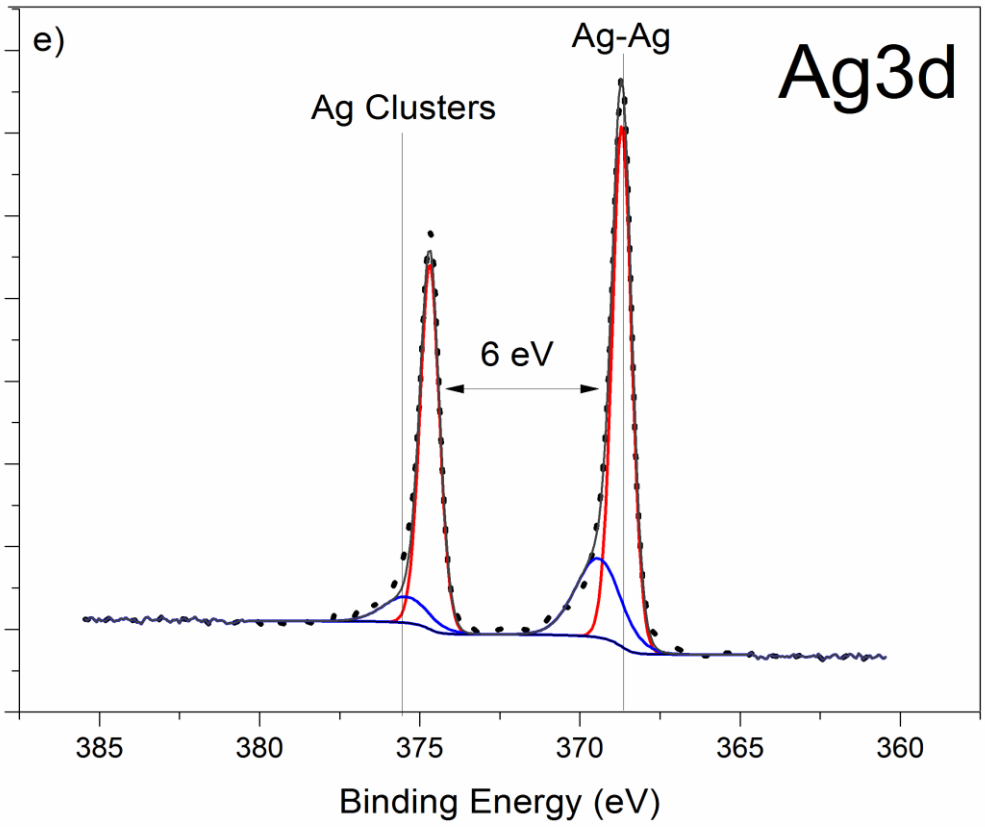

Figure 1.e

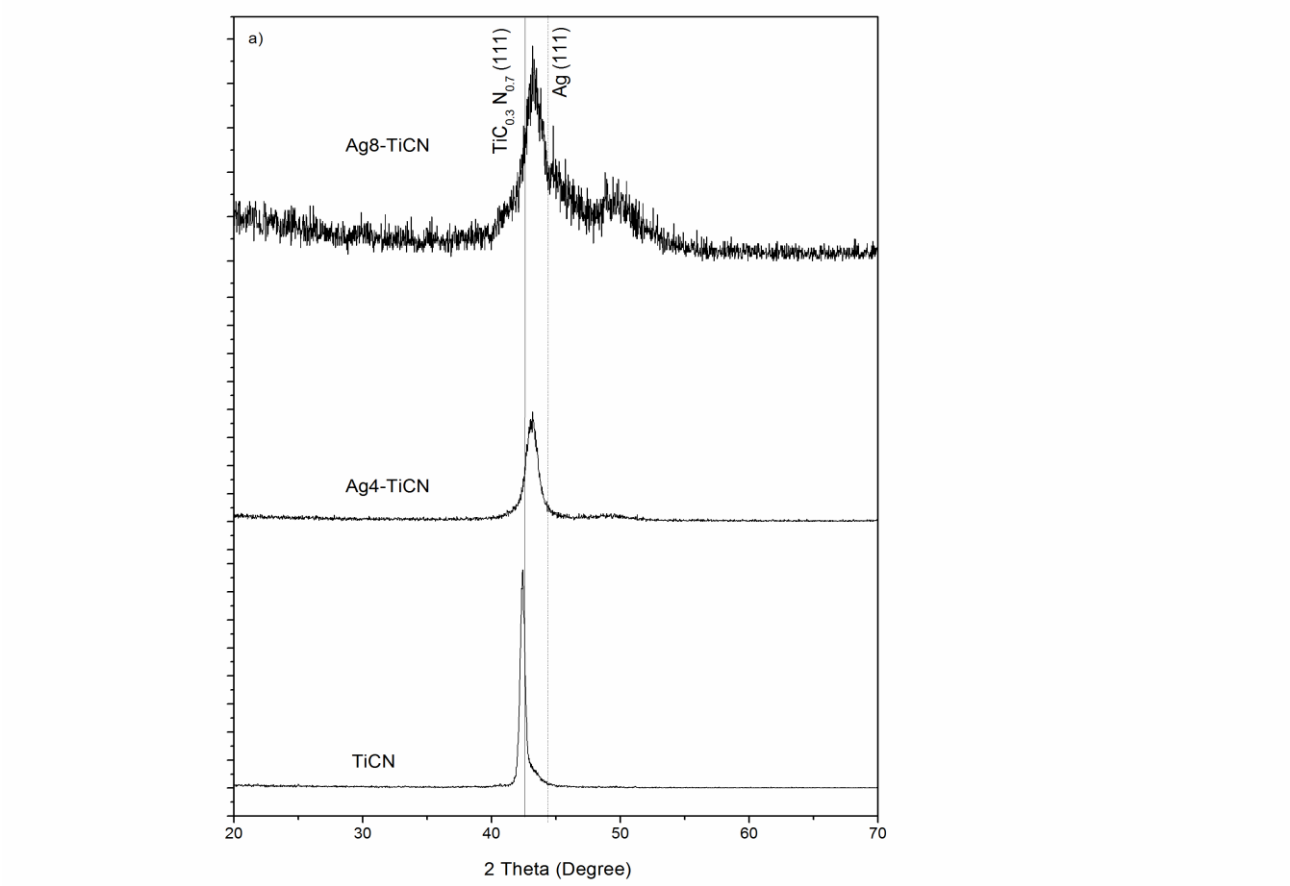

Figure 2.a

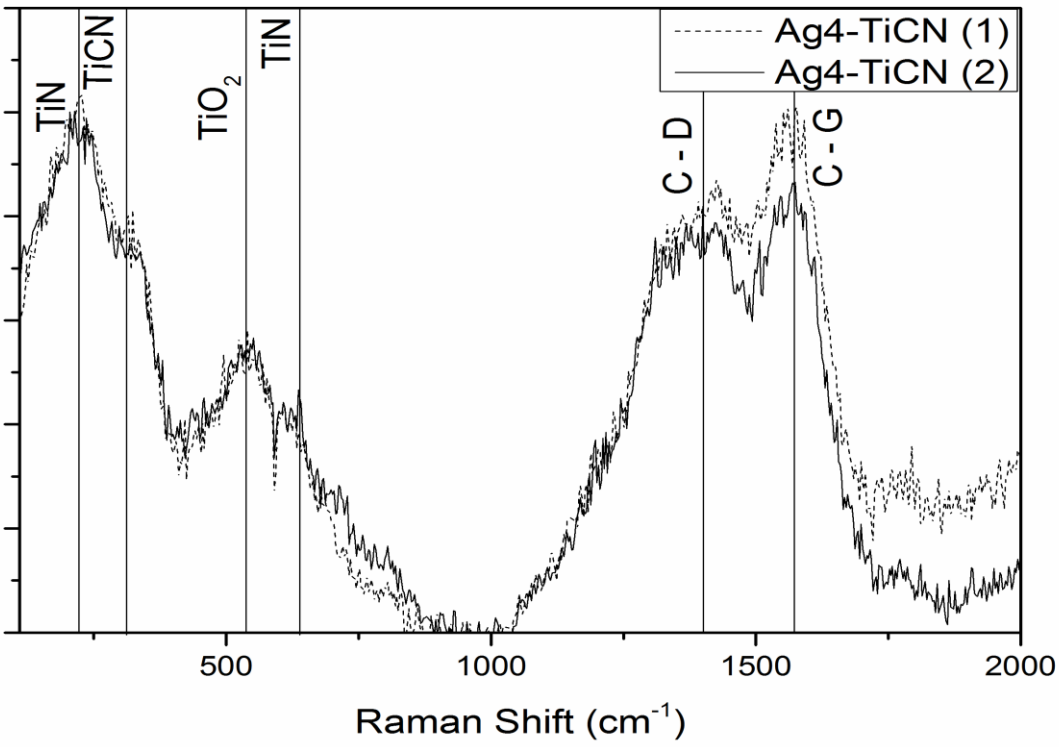

Figure 3

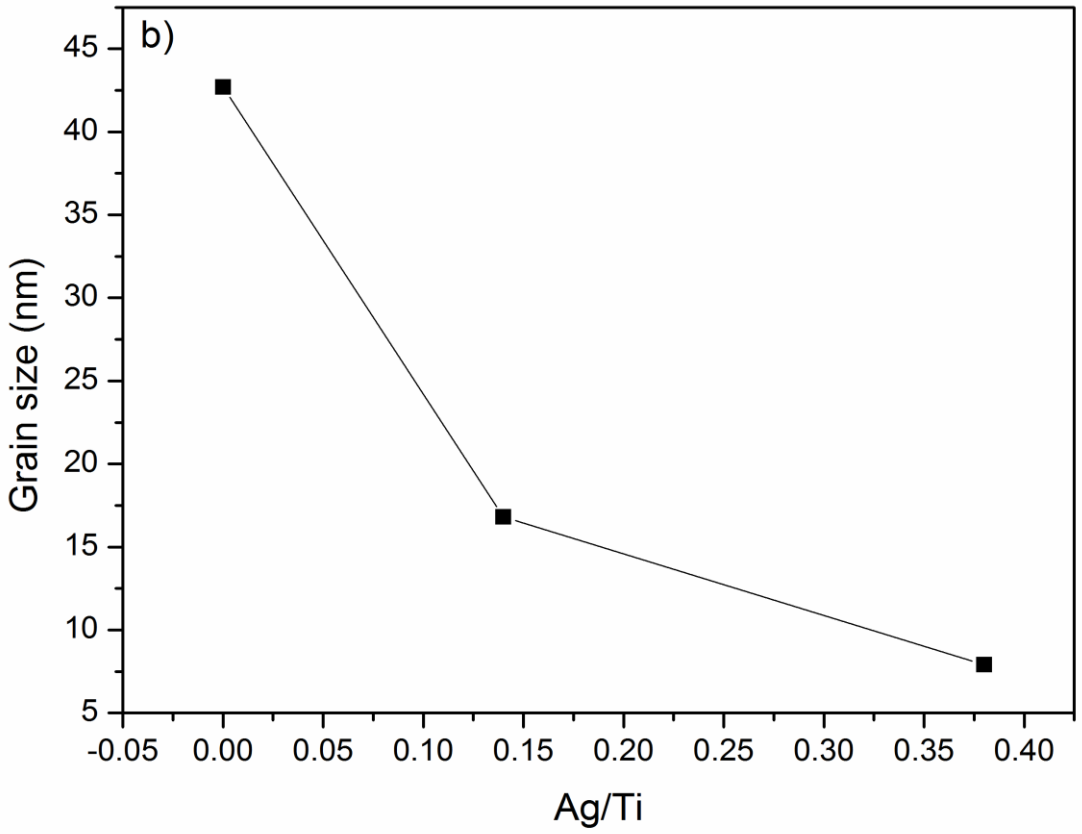

Figure 2.b

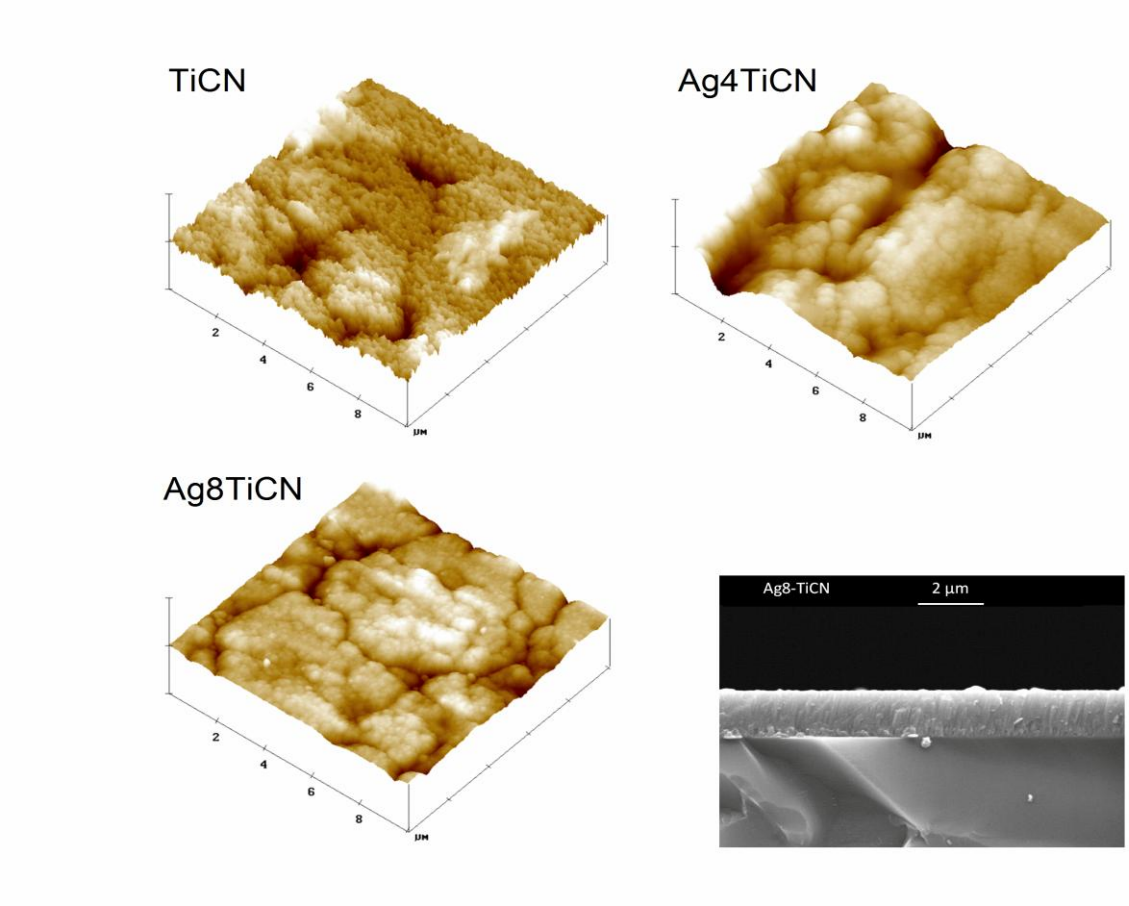

Figure 4

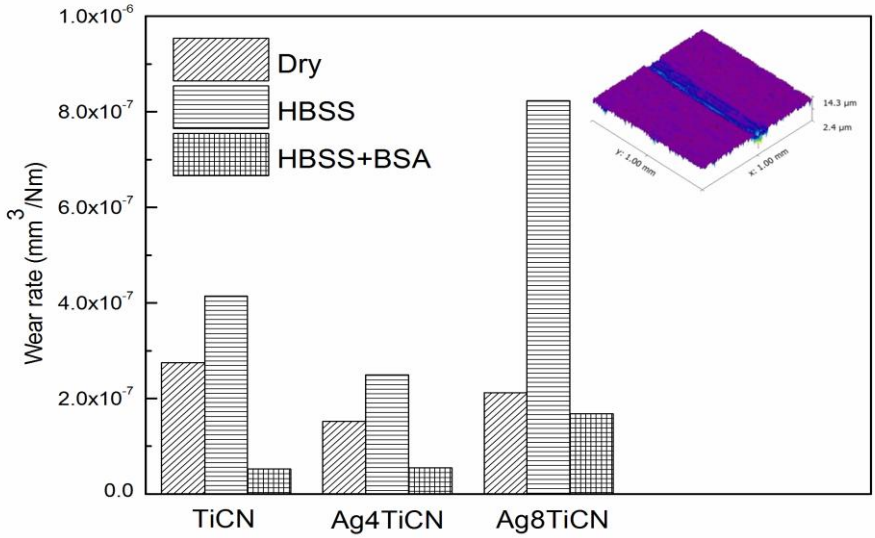

Figure 5

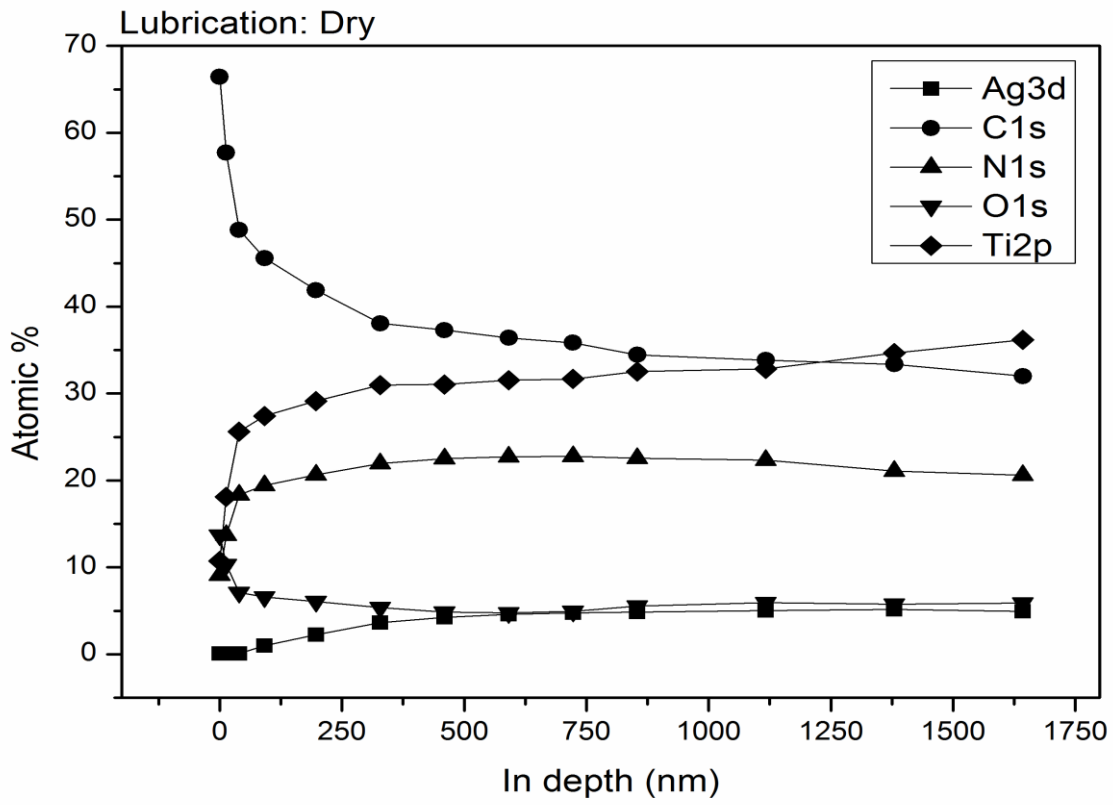

Figure 6

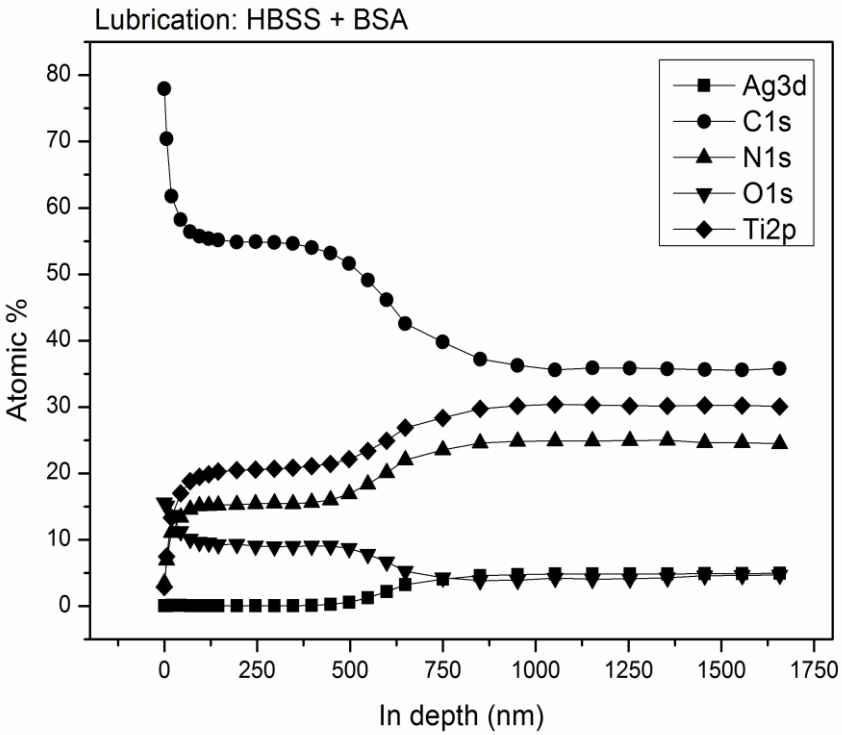

Figure 7